



# Efficient degradation of gaseous benzene by VUV photolysis combined with ozone-assisted catalytic oxidation: Performance and mechanism



Huiling Huang<sup>a</sup>, Haibao Huang<sup>a,b,\*</sup>, Yujie Zhan<sup>a</sup>, Gaoyuan Liu<sup>a</sup>, Xuemei Wang<sup>a</sup>, Haoxian Lu<sup>a</sup>, Liang Xiao<sup>a</sup>, Qiuyu Feng<sup>a</sup>, Dennis Y.C. Leung<sup>c,\*\*</sup>

<sup>a</sup> School of Environmental Science and Engineering, Sun Yat-Sen University, China

<sup>b</sup> Guangdong Provincial Key Laboratory of Environmental Pollution Control and Remediation Technology, Sun Yat-sen University, China

<sup>c</sup> Department of Mechanical Engineering, The University of Hong Kong, Pokfulam Road, Hong Kong

## ARTICLE INFO

### Article history:

Received 19 October 2015

Received in revised form

25 December 2015

Accepted 31 December 2015

Available online 6 January 2016

### Keywords:

Benzene

VUV photolysis

Ozone-assisted catalytic oxidation

Mn/ZSM-5

Degradation mechanism

## ABSTRACT

Vacuum ultraviolet (VUV) photolysis is a simple way to destroy volatile organic compounds (VOCs). However, its application is greatly limited by the formation of O<sub>3</sub> byproduct and the low degradation capacity. In this study, we are the first combining an efficient Mn/ZSM-5 catalyst with VUV photolysis to eliminate O<sub>3</sub> and improve VOC degradation efficiency via ozone-assisted catalytic oxidation (OZCO). Results indicate that the benzene removal efficiency is only 48% with 83 ppm residual O<sub>3</sub> in the VUV photolysis process. However, both benzene and O<sub>3</sub> were completely removed after the adoption of the Mn/ZSM-5 catalyst. O<sub>3</sub> can be efficiently decomposed by Mn/ZSM-5 and used for benzene degradation through the OZCO. The possible degradation pathways and mechanism in such a novel VUV-OZCO process was proposed according to the identified products and intermediates. This study provides an efficient and promising process and unique insights for the degradation of VOCs.

© 2016 Elsevier B.V. All rights reserved.

## 1. Introduction

In recent years, serious haze pollution frequently appeared in rapidly developing economic regions such as India and China [1]. It is a great threat to the atmospheric environment, the ecosystem as well as people living in these regions. Volatile organic compounds (VOCs) have proven to be one of the vital precursors to the formation of fine particulate matter and photochemical smog [2,3]. Besides the atmospheric environmental risk, many VOCs, such as benzene, toluene and formaldehyde, are carcinogenic and detrimental to the public health and safety [4]. Compared with other air pollutants like SO<sub>2</sub> and NO<sub>x</sub>, VOCs are characterized as complex structures, widely available resources and diversity. It is difficult to develop efficient methods to reduce VOCs emission. Many attempts have been made to remove VOCs, including adsorption [5], catalytic combustion [6,7], biological degradation [8], and non-thermal plasma [9]. However, these methods still can't meet the increasingly stringent discharge standards due to their intrinsic

limitations and the diversity of VOCs. For example, the adsorption method only transfers VOCs from a gas phase to an adsorbent that needs further disposal or frequent regeneration. Catalytic combustion is greatly limited by an expensive noble metal catalyst and excessive energy consumption. It also has a risk of catalytic deactivation and VOCs explosion at high temperature [10]. Photocatalytic oxidation (PCO) is generally regarded as an innovative and promising process to degrade low-concentration VOCs since it can proceed at room temperature. However, its application is greatly limited by catalytic deactivation, low efficiency and electron-hole pair recombination [11–13].

Recently, vacuum ultraviolet (VUV) photolysis has attracted some attention since it is a simple method of VOC abatement. A VUV lamp emits UV light at a wavelength of 185 nm and generates energetic photons that can activate oxygen and water vapor to produce numerous reactive species such as O(<sup>1</sup>D), O(<sup>3</sup>P), hydroxyl radicals (<sup>•</sup>OH) and O<sub>3</sub> [14,15]. VUV photolysis has been used to destruct various VOCs including benzene [16], toluene and methylbenzene [17]. Nevertheless, this process is greatly restricted by the low degradation capacity and mineralization rate for VOC destruction [18,19]. Worst of all, large quantities of residual O<sub>3</sub> remains in the exhaust, which brings new air pollution [20,21]. O<sub>3</sub> at levels as low as 0.1–1 ppm can still be harmful to human health by causing headaches, dry throat, and damage to mucus membranes

\* Corresponding author at: School of Environmental Science and Engineering, Sun Yat-sen University, China. Fax: +86 2039336475.

\*\* Corresponding author.

E-mail addresses: [seabao8@gmail.com](mailto:seabao8@gmail.com), [huanghb6@mail.sysu.edu.cn](mailto:huanghb6@mail.sysu.edu.cn) (H. Huang), [yicleung@hku.hk](mailto:yicleung@hku.hk) (D.Y.C. Leung).

[22]. Some attempts have been made to improve the degradation capacity of VOCs using VUV as irradiation sources of photocatalytic oxidation [15,23]. Unfortunately, photocatalysts were generally not efficient in  $O_3$  decomposition and the  $O_3$  byproduct still presented a big challenge to its usage. It is critical for the VUV photolysis process to completely eliminate its residual  $O_3$ .

Meanwhile,  $O_3$  is well known as a strong oxidant. This is significant if  $O_3$  can be decomposed and enhance VOC oxidation during its decomposition. Although direct oxidation of VOCs by  $O_3$  alone can hardly proceed,  $O_3$  becomes highly active for VOC oxidation with the assistance of catalysts [24–26]. Transition metal oxides are the most studied catalysts for  $O_3$  decomposition, and among these oxides exhibited superior catalytic activity [27,28]. It would be highly interesting to combine VUV photolysis with ozone-assisted catalytic oxidation (OZCO). Such a novel process was expressed as VUV-OZCO, in which VOCs would be initially destructured by the VUV photolysis and then be further oxidized by the OZCO using the residual  $O_3$  from the VUV photolysis.  $O_3$  was removed and used to further enhance VOC degradation simultaneously.

In this study, ZSM-5 was used to support  $MnO_x$  due to its mesoporous structure and large specific surface area, which is beneficial not only to the dispersion of metal oxides but also to the adsorption of VOCs and ozone [26,29]. The developed  $MnO_x$ /ZSM-5 combined well with VUV to eliminate  $O_3$  and degrade benzene, a representative toxic VOC. The products and intermediates from benzene degradation were analyzed and used to propose the possible pathways and mechanism of the VUV-OZCO process.

## 2. Experimental methods

### 2.1. Experimental set-up

Fig. 1 shows the schematic diagram of the VUV-OZCO system used in the present study. It consists of a gas distribution system, a VUV-OZCO reactor and gas analyzers. The gas generated from the zero air generator is dry and free of CO and  $CO_2$ . It was used to bubble water and benzene liquid to generate water and benzene vapor, respectively. The benzene concentration, humidity and gas flow can be regulated by three mass flow controllers (S49, Horibametron). A home-made continuous-flow VUV-OZCO reactor includes a VUV photolysis and an OZCO unit. The VUV photolysis unit is composed of two VUV lamps (4 W, Cnlight) placed vertically in a glass tube reactor with effective volume of about 0.5 L. The residual benzene and  $O_3$  from the VUV photolysis flowed into the OZCO unit in which the catalysts were loaded. The concentrations of benzene, and CO and  $CO_2$  generated from benzene oxidation, were measured by gas chromatography (GC) (9790II, Fuli) equipped with two flame-ionization detectors (FID). One FID was connected

with a Rt-Q-BOND PLOT column ( $30m \times 0.25$  mm id, film thickness 10  $\mu$ m) and used for benzene analysis. The injection and detector temperature was 100 °C and 250 °C, respectively. The other FID equipped with a packed column (TDX-01, 3 m  $\times$  3 mm) was followed by a methanizer and used to determine the concentrations of CO and  $CO_2$ . The GC/FID system was calibrated using standard gas. The gas samples from the reaction system were fed on-line to the GC by an automatic gas sampling valve. The gaseous organic intermediates from benzene degradation were directly identified by GC-MS (GRIFFIN 460, LabTech). The solid-phase intermediates deposited on the catalyst were extracted with a  $CS_2$  solution and then identified by GC-MS. The ozone concentration at the outlet was monitored by an ozone analyzer (202, 2B Technology). The flow rate of air containing benzene was 1 L/min. The initial concentration of benzene and relative humidity was fixed at 25 ppm and 50%, respectively. One gram of catalyst with 20–40 mesh was used in the test.

### 2.2. Catalyst preparation

ZSM-5 molecular sieves (Si/Al = 200, Nankai University) served as a catalyst carrier to support  $MnO_x$  by impregnation method. The Mn/ZSM-5 was prepared via the following procedures: 0.803 g manganese acetate was dissolved in the 6 mL deionized water and 3 g ZSM-5 powder was added into the solution while stirring. After impregnation for 12 h, the slurry was dried in an oven at 110 °C for 12 h, and then calcined in air at 550 °C for 3 h. The obtained Mn/ZSM-5 powders were ground up, tableted, crushed, and sieved to 20–40 mesh. The as-prepared catalyst was named as Mn/ZSM-5. The calculated loading of Mn on ZSM-5 was 6% (w.t.).

### 2.3. Catalyst characterization

The surface area and pore volume of the catalyst produced were determined through a  $N_2$  adsorption/desorption analysis conducted at 77 K on a Micromeritics Tristar II 3020 system. The specific surface area was calculated by the BET method. The size and morphology of the as-synthesized catalysts were recorded by a scanning electron microscope (SEM) (400F, Quanta) and a transmission electron microscope (TEM) (Tecnai G2 Spirit, FEI). The loading of the metal Mn was measured by inductively coupled plasma (ICP, 4300 DV, PerkinElmer). The Mn valence states in the samples were determined by X-ray photoelectron spectroscopy (XPS) with a spectrometer (ESCALAB 250, Thermo Fisher Scientific) performed with a monochromatic Al K $\alpha$  X-ray source. During XPS measurements, the base pressure of the sample chamber was kept below  $2.0 \times 10^{-9}$  mbar. Emission lines were calibrated with the  $C_{1s}$  signal at 284.8 eV.

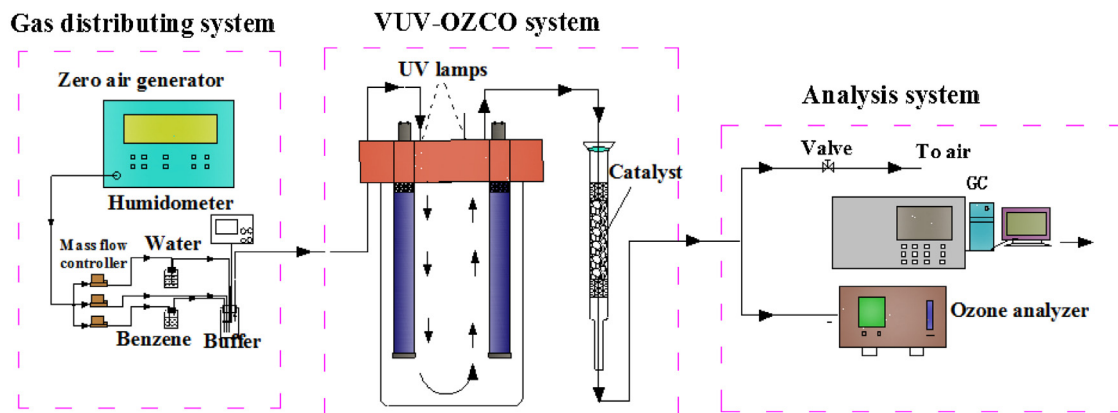
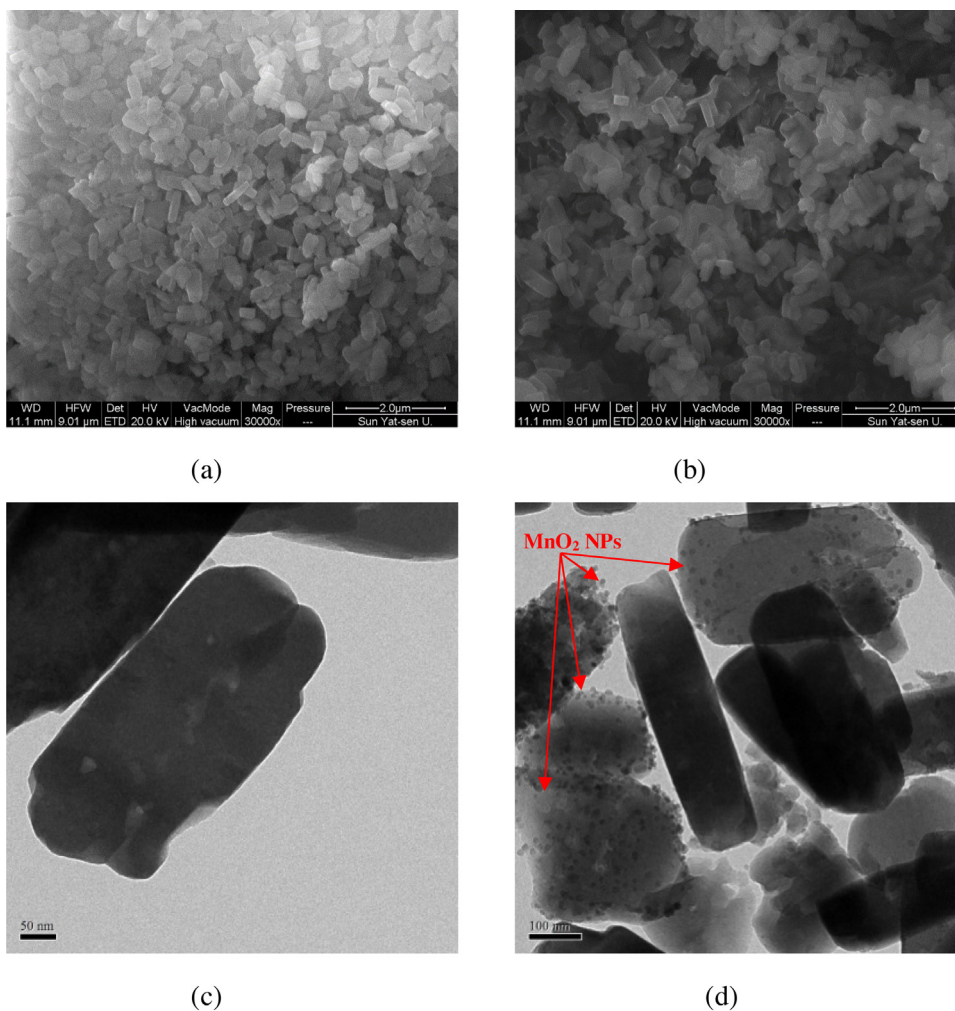


Fig. 1. The schematic diagram of the VUV-OZCO system.



**Fig. 2.** SEM images: (a) ZSM-5, (b) Mn/ZSM-5; TEM images: (c) ZSM-5, and (d) Mn/ZSM-5.

### 3. Results and discussion

#### 3.1. Catalyst characterization

The morphology of the catalysts was observed using the SEM. As shown in Fig. 2a and b, both pure ZSM-5 (top left) and Mn/ZSM-5 (top right) particles were uniformly rod-like and the crystalline sizes ranged from 400 nm to 500 nm. No remarkable changes were observed in the size of ZSM-5 particles over the Mn/ZSM-5 while its surface was covered with MnO<sub>x</sub>. The TEM operation was used to further observe the distribution of MnO<sub>x</sub>, as shown in Fig. 2c and d. The TEM patterns (bottom left) suggest that the ZSM-5 catalyst surface is smooth. The MnO<sub>x</sub> nanoparticles (NPs), with a mean size of 10–20 nm, were highly uniformly distributed on the surface of the Mn/ZSM-5 (bottom right), and no significant reunion was found.

The BET surface area and pore volume of the ZSM-5 and Mn/ZSM-5 catalysts are shown in Table 1. The specific surface area of ZSM-5 reached a high value of 373.2 m<sup>2</sup>/g, which contributes to the high dispersion of MnO<sub>x</sub> nanoparticles, as observed by the TEM in Fig. 2. The BET surface area of the Mn/ZSM-5 dropped by ~16%

**Table 1**  
Textural characteristics of ZSM-5 and Mn/ZSM-5.

Catalysts	BET surface area, m <sup>2</sup> /g	Pore volume (cm <sup>3</sup> /g)	Mn content (%)
ZSM-5	373.2	0.23	–
Mn/ZSM-5	314.6	0.22	4.3

to 314.6 m<sup>2</sup>/g due to the partial blockage of pores. The pore volume decreased by ~4% from 0.23 to 0.22 cm<sup>3</sup>/g after Mn deposition over ZSM-5. According to the ICP result, the Mn loading was 4.3%.

XPS was employed to investigate the valence state of Mn of the Mn/ZSM-5 before and after catalytic experiments. As shown in Fig. 3, there were two distinct peaks at binding energies (BEs) of 642.9 and 654.3 eV, while the spin-orbital splitting of 11.4 eV appeared in the Mn 2p core level spectrum of all samples. They were larger than the BEs of Mn<sub>2</sub>O<sub>3</sub> while close in size to that of MnO<sub>2</sub> [30,31], indicating that the obtained MnO<sub>x</sub> mainly existed in the form of MnO<sub>2</sub>. The XPS spectra of Mn after catalytic experiments are similar to those before catalytic experiments, indicating the valence state of Mn remained unchanged after reaction.

#### 3.2. Catalytic activity test

The performance of benzene degradation under different processes was compared. As shown in Fig. 4, benzene removal efficiency increased in the order of VUV < VUV-OZCO (ZSM-5) < VUV-OZCO (Mn/ZSM-5). It was stably maintained at about 48% for the whole VUV photolysis. As bare ZSM-5 was combined with the VUV photolysis, benzene removal efficiency reached 100% at the initial stage due to the adsorption of ZSM-5, but it gradually decreased after reaction for about 120 min, and eventually dropped to about 50%, which was close to that of VUV alone. This suggested that benzene degradation was mainly ascribed to the VUV

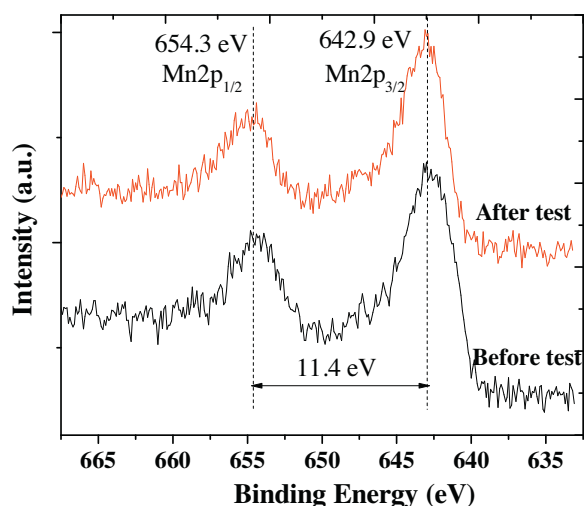


Fig. 3. Mn 2p XPS spectra of Mn/ZSM-5 before and after catalytic experiments.

photolysis in the VUV-OZCO (ZSM-5) and bare ZSM-5 could not effectively use  $O_3$  to improve benzene degradation. In contrast, after the loading of Mn over ZSM-5, benzene removal efficiency was stayed at 100% for a long period in the VUV-OZCO (Mn/ZSM-5) process and reached as high as 95.5% even after reaction for 400 min. The residual benzene after the VUV photolysis further underwent catalytic oxidation in the OZCO unit. In order to clarify the effect of adsorption, the Mn/ZSM-5 catalyst was used to adsorb residual benzene free of  $O_3$ . Mn/ZSM-5 broke through after benzene adsorption for about 60 min, roughly twice as fast as the VUV-OZCO (Mn/ZSM-5) process. It was completely saturated after adsorption for about 360 min. Mn/ZSM-5 demonstrated a good capacity for benzene adsorption, which is critical to the benzene OZCO reaction.

In order to confirm the oxidation of benzene in the process, the  $CO_x$  concentration in the outlet stream was measured. Fig. 5 shows the concentration of CO or  $CO_2$  generated from benzene degradation under different processes. No CO and  $CO_2$  was produced during the adsorption, indicating that no benzene was oxidized. As for the VUV-OZCO (ZSM-5), the outlet CO and  $CO_2$  reached 22 and 38 ppm, respectively, which was close to the same values from the VUV photolysis. These results also demonstrated that the benzene degradation is mainly attributed to the VUV photolysis. As for the

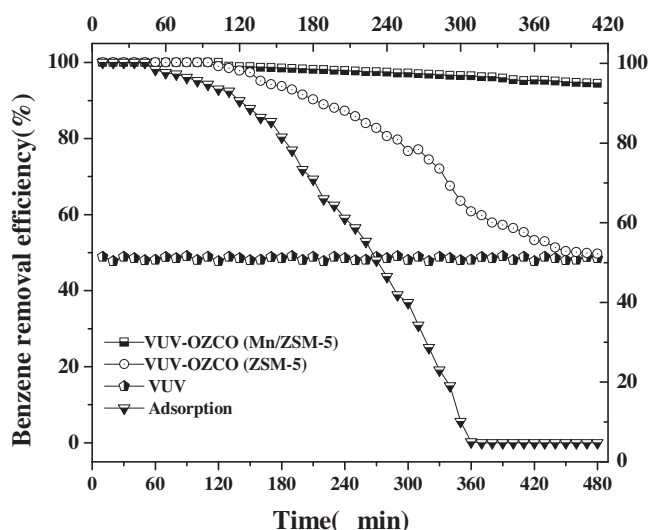


Fig. 4. Benzene removal efficiency under different processes.

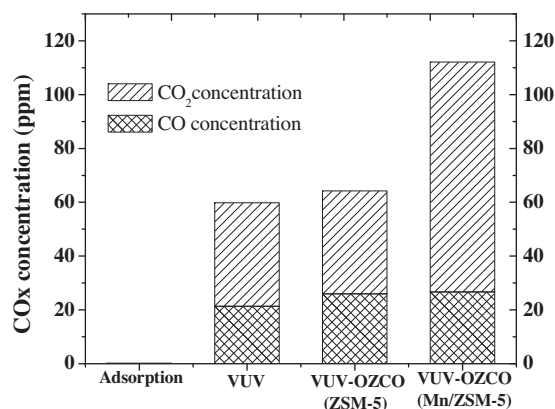


Fig. 5. The  $CO_x$  concentration under different processes.

VUV-OZCO (Mn/ZSM-5), CO concentrations were close to that of the VUV photolysis, while  $CO_2$  concentrations greatly increased to 85.5 ppm, which was more than twice of the VUV alone. The residual benzene from the VUV photolysis was mainly oxidized into  $CO_2$  and nearly no additional CO was generated in the OZCO unit with the Mn/ZSM-5, leading to better benzene mineralization. Bare ZSM-5 can hardly promote benzene degradation, but the introduction of Mn into ZSM-5 significantly improved the removal efficiency and mineralization rate of benzene.

$O_3$  byproduct presents a big challenge for the VUV photolysis of VOCs. The  $O_2$  in the air absorbed UV irradiation of wavelength 185 nm, generating a strong oxidant,  $O_3$  [32]. Fig. 6 shows the outlet ozone concentration changes under different processes. The residual  $O_3$  concentration after the VUV photolysis was about 83 ppm. The  $O_3$  concentration initially reduced to 12.1 ppm but then gradually increased as pure ZSM-5 was combined with the VUV photolysis. Although some  $O_3$  decomposed, this process did not contribute to benzene oxidation, as previously described in Figs. 4 and 5. This suggests that  $O_3$  from the VUV photolysis was not fully used by the ZSM-5. In contrast, the  $O_3$  concentration was kept at 0 ppm throughout the reaction in the VUV-OZCO (Mn/ZSM-5) process, indicating that the Mn/ZSM-5 is highly efficient for  $O_3$  decomposition. The residual  $O_3$  decomposed and was used to oxidize benzene by the Mn/ZSM-5 in the OZCO unit. Compared with pure ZSM-5, Mn/ZSM-5 showed a much better catalytic activity towards  $O_3$  decomposition and benzene degradation possibly because the Mn oxide can interact with Lewis acid or alkali sites, resulting in the tenability of electron density of Mn

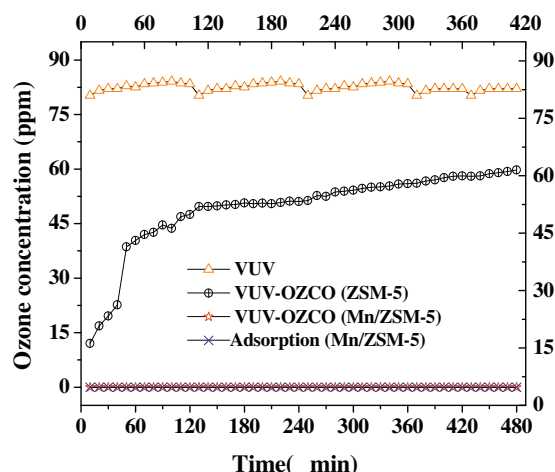


Fig. 6. The outlet  $O_3$  concentration under different processes.



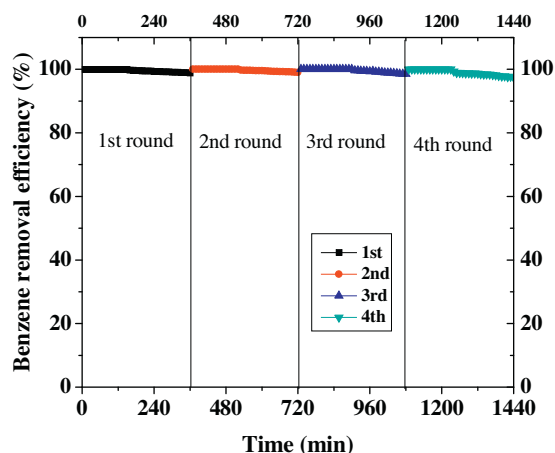


Fig. 7. Catalytic stability of the VUV-OZCO(Mn/ZSM-5) for benzene removal.

ions, thus enhancing the ability of Mn species involved in the redox cycle and ultimately increasing the oxidation activity of the catalyst [33]. As shown in the TEM images in Fig. 2d,  $\text{MnO}_x$  nanoparticles were highly dispersed on ZSM-5, which provided numerous catalytic sites for  $\text{O}_3$  decomposition and benzene degradation. In addition, the Mn/ZSM-5 had a high BET surface area and good benzene adsorption capacity, which also contributed to its excellent catalytic activity [34,35].

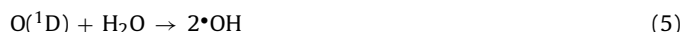
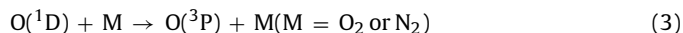
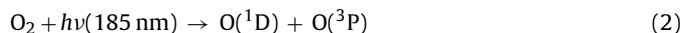
### 3.3. Catalytic stability test

As shown in Fig. 4, Mn/ZSM-5 exhibited good catalytic activity during the VUV-OZCO, but the benzene removal efficiency slightly decreased as the reaction proceeded. In order to study its catalytic stability, the test was performed four times under the same conditions. After each run for 6 h, the Mn/ZSM-5 was dried for 2 h under  $150^\circ\text{C}$  for regeneration. Fig. 7 shows that the catalytic activity nearly recovered after regeneration, indicating that such slight deactivation is reversible and easily regenerated. No  $\text{O}_3$  was detected in any of the runs. These results show that Mn/ZSM-5 demonstrates superior catalytic stability toward benzene oxidation and  $\text{O}_3$  elimination, which is important for its potential application.

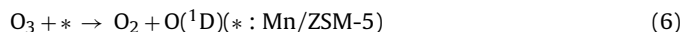
### 3.4. Mechanistic study

Benzene degradation consisted of two stages in the VUV-OZCO process, i.e., VUV photolysis and subsequent OZCO. The proposed schematic of benzene oxidation in the VUV-OZCO process is shown in Fig. 8.

During the VUV photolysis stage, some reactions are involved in the formation of active species such as  $\text{O}(^1\text{D})$ ,  $\bullet\text{OH}$  and  $\text{O}_3$  [14,15]:



The  $\text{O}(^1\text{D})$  and  $\bullet\text{OH}$  are highly active for benzene degradation. In the VUV photolysis stage, nearly 48% of benzene was removed and most of this was oxidized into CO and  $\text{CO}_2$ .  $\text{O}_3$  was also generated in this stage, though it could not directly oxidize benzene but was supplied for the OZCO unit.  $\text{O}_3$  was catalytically decomposed by the Mn/ZSM-5 in the OZCO unit to generate active species via the following steps [36,37]:



Both benzene and  $\text{O}_3$  was transferred to the surface of the Mn/ZSM-5 and  $\text{MnO}_x$  acted as the active sites for  $\text{O}_3$  decomposition and benzene oxidation. All the residual benzene was removed in the OZCO stage and most of this was oxidized into  $\text{CO}_2$ .

If all the initial benzene (25 ppm) was completely mineralized into CO or  $\text{CO}_2$ , 150 ppm  $\text{CO}_x$  would be formed. However, the sum of CO and  $\text{CO}_2$  concentration is less than 120 ppm (as shown in Fig. 5), indicating that some trace intermediates were generated from benzene degradation. The organic intermediates in gas-phase and on the surface of the catalyst were identified by the GC–MS and are listed in Table 2.

It has been reported that benzene could dehydrogenate under irradiation of UV with wavelength less than 200 nm, leading to the opening of the benzene ring and formation of unsaturated hydrocarbon [38]. Such unsaturated hydrocarbon was reduced by reactive hydrogen and then reacted with methyl, generating saturated hydrocarbon substances such as nonane, decane and octane, which were identified by the GC–MS. The broken benzene ring was oxidized to generate aldehydes by oxidants [39], and then further oxidized into acid substance. In this study, decanal and decanoic acid was identified by the GC–MS. Only *p*-benzoquinone was identified in solid-phase and it should be generated from the OZCO unit. It has been reported that benzene can be firstly oxidized by  $\bullet\text{OH}$  to form phenol, which can further oxidize to, eventually form *p*-benzoquinone [40,41]. The VUV-OZCO was composed of the VUV photolysis and the OZCO processes. The trace hydrocarbon intermediates including octane, aldehydes, nonane, and decane should be generated by the VUV photolysis and other intermediates should

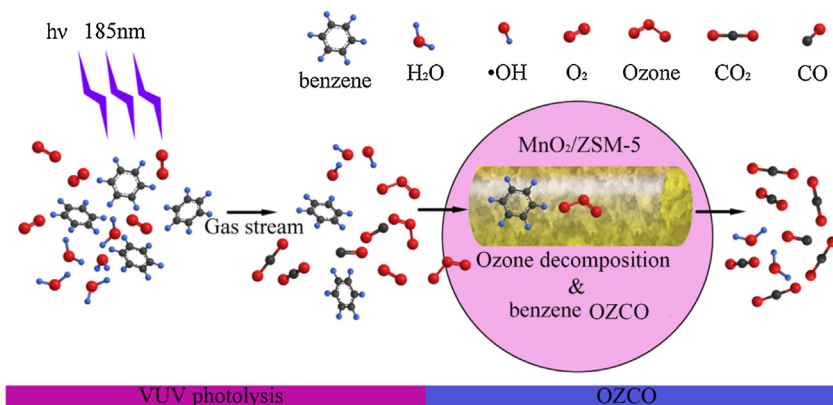
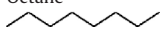




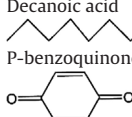
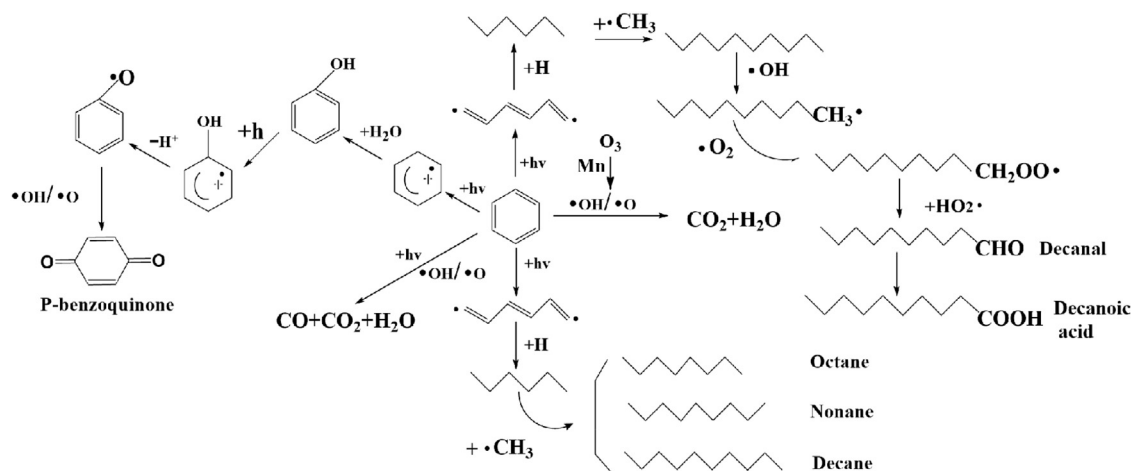


Fig. 8. The schematic of benzene oxidation in the VUV-OZCO process over the Mn/ZSM-5 catalyst.

**Table 2**  
Intermediates of benzene degradation by the VUV-OZCO

Intermediates and its structure	Gas-phase	Solid-phase
Octane 	✓	–
Decane 	✓	–
Nonane 	✓	–
Decanal 	✓	–
Decanoic acid 	✓	–
P-benzoquinone 	–	✓

Note: ✓: Detected; –: undetected.



**Fig. 9.** Degradation mechanism of benzene molecule under VUV-OZCO process.

be ascribed to the reactive oxidants generated in both the VUV photolysis and OZCO stages. According to the identified products and by-products, the possible pathway of benzene degradation in the VUV-OZCO was proposed in Fig. 9.

#### 4. Conclusions

It is the first study combining an efficient Mn/ZSM-5 catalyst with VUV photolysis to eliminate  $O_3$  and enhance VOC degradation via ozone-assisted catalytic oxidation (OZCO). The benzene removal efficiency only reached 48% with 83 ppm residual  $O_3$  in the VUV photolysis process, but benzene and  $O_3$  were both completely removed after combined with the Mn/ZSM-5. This study reveals that  $O_3$  can be efficiently decomposed by the Mn/ZSM-5 and used for benzene degradation through the OZCO. The possible degradation pathways and mechanism in such a novel VUV-OZCO process was proposed according to the identified products. This study provides an efficient and potential process with promising insights for the degradation of VOCs.

#### Acknowledgements

The authors gratefully acknowledge the financial supports from National Nature Science Foundation of China (No. 51208207), Doctoral Program of Higher Education of China (No. 20120172120039), Science and Technology Project in Guangzhou (No.2014Y2-00094), NSFC-RGC (No. 51561165015, No. N.HKU718/15), and the Key Fundamental Research Funds for the Central Universities (15lgic07).

#### References

- [1] X. Zhang, L. Wang, W. Wang, D. Cao, X. Wang, D. Ye, *Atmos. Environ.* 119 (2015) 362–373.
- [2] J. Zheng, Y. Yu, Z. Mo, Z. Zhang, X. Wang, S. Yin, K. Peng, Y. Yang, X. Feng, H. Cai, *Sci. Total Environ.* 456–457 (2013) 127–136.
- [3] R. Volkamer, L.T. Molina, M.J. Molina, T. Shirley, W.H. Brune, *Geophys. Res. Lett.* 32 (2005) L08806.
- [4] C.A. Korologos, M.D. Nikolaki, C.N. Zerva, C.J. Philippopoulos, S.G. Pouloupoulos, *J. Photochem. Photobiol. A: Chem.* 244 (2012) 24–31.
- [5] S. Standeker, Z. Novak, Z. Knez, *J. Hazard. Mater.* 165 (2009) 1114–1118.
- [6] F.I. Khan, A. Kr. Ghoshal, *J. Loss Prev. Process Ind.* 13 (2000) 527–545.
- [7] S. Chavadej, W. Kiatubolpaiboon, P. Rangsunvigit, T. Sreethawong, *J. Mol. Catal. A: Chem.* 263 (2007) 128–136.
- [8] K. Urashima, J.-S. Chang, *IEEE Trans. Dielectr. Electr. Insul.* 7 (2000) 602–614.
- [9] H. Huang, D. Ye, D.Y. Leung, F. Feng, X. Guan, *J. Mol. Catal. A: Chem.* 336 (2011) 87–93.
- [10] H.B. Huang, Y. Xu, Q.Y. Feng, D.Y.C. Leung, *Catal. Sci. Technol.* 5 (2015) 2649–2669.
- [11] J. Mo, Y. Zhang, Q. Xu, Y. Zhu, J.J. Lamson, R. Zhao, *Appl. Catal. B: Environ.* 89 (2009) 570–576.
- [12] H. Huang, W. Li, *Appl. Catal. B: Environ.* 102 (2011) 449–453.
- [13] M.D. Hernández-Alonso, F. Fresno, S. Suárez, J.M. Coronado, *Energy Environ. Sci.* 2 (2009) 1231–1257.
- [14] T. Hashem, M. Zirlwaghen, A. Braun, *Water Sci. Technol.* 35 (1997) 41–48.
- [15] P. Fu, *Appl. Catal. B: Environ.* 105 (2011) 220–228.
- [16] H.B. Huang, H.L. Huang, L. Zhang, P. Hu, Y. Xu, X.G. Ye, X.S. Liang, J.D. Chen, M.Y. Ji, *Environ. Eng. Sci.* 31 (2014) 481–486.
- [17] J. Jeong, K. Sekiguchi, M. Saito, Y. Lee, Y. Kim, K. Sakamoto, *Chem. Eng. J.* 118 (2006) 127–130.
- [18] T. Alapi, A. Dombi, *J. Photochem. Photobiol. A: Chem.* 188 (2007) 409–418.
- [19] J. Zhao, X. Yang, *Build. Environ.* 38 (2003) 645–654.
- [20] L. Yang, Z. Liu, J. Shi, Y. Zhang, H. Hu, W. Shangguan, *Sep. Purif. Technol.* 54 (2007) 204–211.
- [21] T. Alapi, A. Dombi, *Chemosphere* 67 (2007) 693–701.

- [22] H. Huang, D.Y.C. Leung, G. Li, M.K.H. Leung, X. Fu, *Catal. Today* 175 (2011) 310–315.
- [23] P. Fu, *Chin. J. Catal.* 35 (2014) 210–218.
- [24] E. Rezaei, J. Soltan, *Appl. Catal. B: Environ.* 148–149 (2014) 70–79.
- [25] H. Einaga, Y. Teraoka, A. Ogata, *Catal. Today* 164 (2011) 571–574.
- [26] H. Huang, X. Ye, W. Huang, J. Chen, Y. Xu, M. Wu, Q. Shao, Z. Peng, G. Ou, J. Shi, X. Feng, Q. Feng, H. Huang, P. Hu, D.Y.C. Leung, *Chem. Eng. J.* 264 (2015) 24–31.
- [27] E. Saputra, S. Muhammad, H. Sun, H.-M. Ang, M.O. Tadé, S. Wang, *Appl. Catal. B: Environ.* 154–155 (2014) 246–251.
- [28] E. Saputra, S. Muhammad, H. Sun, H.-M. Ang, M.O. Tadé, S. Wang, *Appl. Catal. B: Environ.* 142–143 (2013) 729–735.
- [29] C.W. Kwong, C.Y.H. Chao, K.S. Hui, M.P. Wan, *Atmos. Environ.* 42 (2008) 2300–2311.
- [30] H. Xia, D. Zhu, Z. Luo, Y. Yu, X. Shi, G. Yuan, J. Xie, *Science* (2013) 3.
- [31] Y. Zhang, Z. Qin, G. Wang, H. Zhu, M. Dong, S. Li, Z. Wu, Z. Li, Z. Wu, J. Zhang, T. Hu, W. Fan, J. Wang, *Appl. Catal. B: Environ.* 129 (2013) 172–181.
- [32] J.M. Chen, Z.W. Cheng, Y.F. Jiang, L.L. Zhang, *Chemosphere* 81 (2010) 1053–1060.
- [33] Y. Jin song, *J. Mol. Catal. (China)* 20 (2006) 300–305.
- [34] M. Firoozi, M. Baghalha, M. Asadi, *Catal. Commun.* 10 (2009) 1582–1585.
- [35] M. Uguina, J. Sotelo, D. Serrano, *Appl. Catal.* 76 (1991) 183–198.
- [36] H. Einaga, S. Futamura, *J. Catal.* 243 (2006) 446–450.
- [37] H. Einaga, Y. Teraoka, A. Ogata, *J. Catal.* 305 (2013) 227–237.
- [38] V.V. Kislov, T.L. Nguyen, A.M. Mebel, S.H. Lin, S.C. Smith, *J. Chem. Phys.* 120 (2004) 7008–7017.
- [39] R. Volkamer, U. Platt, K. Wirtz, *J. Phys. Chem. A* 105 (2001) 7865–7874.
- [40] P.P. Olga d'Hennezela, P. Pichat, F. David Ollisb, *J. Photochem. Photobiol. A: Chem.* 118 (1998) 197–204.
- [41] S. Zhang, Z. Zheng, J. Wang, J. Chen, *Chemosphere* 65 (2006) 2282–2288.